International Journal of Nanomedicine

Dovepress
open access to scientific and medical research

Open Access Full Text Article

ORIGINAL RESEARCH

Continuous release of bone morphogenetic protein-2 through nano-graphene oxide-based delivery influences the activation of the NF-κB signal transduction pathway

This article was published in the following Dove Press journal:
International Journal of Nanomedicine
13 February 2017
Number of times this article has been viewed

Cheng Zhong[1]
Jun Feng[2]
Xiangjin Lin[1,*]
Qi Bao[3,4,*]

[1]Department of Orthopaedic, First Affiliated Hospital, School of Medicine, Zhejiang University, Hangzhou, People's Republic of China; [2]Department of Molecular and Medical Pharmacology, University of California, Los Angeles, CA, [3]Department of Plastic and Reconstructive Surgery, Second Affiliated Hospital, School of Medicine, [4]Institute of Gastroenterology, Zhejiang University, Hangzhou, People's Republic of China

*These authors contributed equally to this work

Abstract: Graphene oxide (GO) has been used as a delivery vehicle for small molecule drugs and nucleotides. To further investigate GO as a smart biomaterial for the controlled release of cargo molecules, we hypothesized that GO may be an appropriate delivery vehicle because it releases bone morphogenetic protein 2 (BMP2). GO characterization indicated that the size distribution of the GO flakes ranged from 81.1 nm to 45,749.7 nm, with an approximate thickness of 2 nm. After BMP2 adsorption onto GO, Fourier-transformed infrared spectroscopy (FTIR) and thermal gravimetric analysis were performed. Compared to GO, BMP2-GO did not induce significant changes in the characteristics of the materials. GO continuously released BMP2 for at least 40 days. Bone marrow stem cells (BMSCs) and chondrocytes were treated with BMP2-GO in interleukin-1 media and assessed in terms of cell viability, flow cytometric characterization, and expression of particular mRNA. Compared to GO, BMP2-GO did not induce any significant changes in biocompatibility. We treated osteoarthritic rats with BMP2 and BMP2-GO, which showed significant differences in Osteoarthritis Research Society International (OARSI) scores ($P<0.05$). Quantitative assessment revealed significant differences compared to that using BMP2 and BMP2-GO ($P<0.05$). These findings indicate that GO may be potentially used to control the release of carrier materials. The combination of BMP2 and GO slowed the progression of NF-κB-activated degenerative changes in osteoarthritis. Therefore, we infer that our BMP2-GO strategy could alleviate the NF-κB pathway by inducing continuous BMP2 release.

Keywords: graphene oxide, BMP2, controlled release, anti-inflammatory

Introduction

Osteoarthritis (OA) is a degenerative joint disease that leads to the destruction of cartilage, followed by reactive hyperplasia of articular cartilage edge, and formation of osteophytes.[1] Age, obesity, strain, joint trauma, congenital abnormality, and joint deformity are risk factors for OA.[2] Treatment of more advanced stages of OA may involve artificial joint replacement, which is currently recognized as the most effective method that could significantly improve the quality of life of patients.[3]

Normal bone morphogenetic protein 2 (BMP2) is an important protein component that is involved in the maintenance of the structure and function of cartilage.[4] BMP2 expression significantly increases during cartilage damage.[5] Thus, it is an important function of BMP2 to maintain the formation of articular cartilage and repair damaged cartilage.[6] Inappropriate BMP2 dosages often cause side effects and raise the costs

Correspondence: Qi Bao
Department of Plastic and Reconstructive Surgery, Second Affiliated Hospital, School of Medicine, Zhejiang University, Jiefang Road 88, Hangzhou 310009, People's Republic of China
Email baoqi@zju.edu.cn

Xiangjin Lin
Department of Orthopaedic, First Affiliated Hospital, School of Medicine, Zhejiang University, Qingchun Road 79, Hangzhou 310003, People's Republic of China
Email zdyygk@126.com

submit your manuscript | www.dovepress.com
Dovepress
http://dx.doi.org/10.2147/IJN.S124040

of treatment programs after surgery. Serious complications such as immune responses, ectopic bone formation, swelling of surgical site, postoperative tissue injury, and osteolysis are caused by inappropriate administration of BMP2.[7,8] Therefore, it is necessary to appropriately administer BMP2 to avoid these complications.[9]

The optimal administration model for BMP2 for the restoration of cartilage is dependent on its delivery vehicle. A number of delivery vehicles that release BMP2 have been evaluated, which include fibrin gels,[10] poly(lactic-co-glycolic acid) (PLGA),[11] chitosan,[12] PLGA nanospheres,[13] and hydrogels.[14] The ideal vehicle should reduce BMP2 usage for cartilage protection. Graphene oxide (GO) has been employed as an in vivo delivery vehicle for small molecule drugs and nucleotides because of its steady biocompatibility,[15] low toxicity,[16] and excellent loading capacity.[9,17] One essential characteristic of GO is its hydrophobic π domains in the core, which are ionized along the edges.[18] GO is a flat monolayer of carbon atoms in a two-dimensional (2D) honeycomb-like structure.[19] Graphene consists of a six-membered ring π-conjugated monolayer, planar aromatic polymer[20] that facilitates binding of a large number of substances, including metals, drugs, biological molecules, fluorescent probes, and cells.[21–24] GO has a large specific surface area, strong ion exchange capacity, and contains a large number of carboxyl-, hydroxyl-, and oxygen-containing functional groups, and thus it has good biocompatibility and high drug-loading capacity. The specific surface area of graphene is 2,600 $m^2 \cdot g/L$, which is fivefold higher than that of nanomaterials currently used in drug delivery.[25] In addition, the oxygen atoms in the six-element ring can form hydrogen bonds with drug molecules, which in turn circumvents molecular aggregation and improves drug efficacy.[26,27]

In the present study, we investigated whether GO as a vehicle for BMP2 improves the BMP2 effect on cartilage protection. The findings of this study may further expand the applications of GO to the biomedical field, which includes utilization as a novel treatment scheme for osteoarthritis.

Materials and methods

Cell culture

Rat bone marrow stem cells (BMSCs) and chondrocytes were purchased from the Institute of Biochemistry and Cell Biology, CAS (Shanghai, China) and cultured in Dulbecco's Modified Eagle's Medium (DMEM; GibcoBRL, Gaithersburg, MD, USA) supplemented with 10% (v/v) fetal bovine serum (FBS, Gibco, Thermofisher Scientific, Waltham, MA, USA). The medium was replaced every 2 days. BMSCs after four passages were used in the experiments. Chondrocytes after three passages were used in the experiments. All the cells were kept at 37°C.

GO characterization

GO flakes were purchased from Chengdu Organic Chemicals Co., Ltd. Chinese Academy of Science (Chengdu, China) and examined by scanning electron microscopy (SEM, JSM-6701F; JEOL, Tokyo, Japan) after platinum coating. The samples were observed under a scanning electron microscope (Hitachi S3000N) at an accelerating voltage of 15 kV. The size distribution of the GO flakes was determined using a zeta electric potential-based spectrophotometer (Zetasizer3000HSA; Malvern Instruments, Malvern, UK). The thickness of the GO flakes was determined by atomic force microscopy (AFM, MultiMode; Veeco, Santa Barbara, CA, USA) coupled with an inverted microscope (IX71 inverted microscope; Olympus, Tokyo, Japan). Thermal gravimetric analysis and differential scanning calorimetry were performed by using a Thermogravimetric Analyzer (TGA)/Differential Scanning Calorimeter (DSC) thermal gravimetric analyzer (Pyris 1 TGA; Perkin-Elmer, Waltham, MA, USA), which involved placing the samples in aluminum pans, which were then heated from 25°C to 1,100°C at a rate of 10°C/min.

BMP2 adsorption onto GO

GO flakes were labeled with 1,1-dioctadecyl-3,3,3,3-tetramethylindocarbocyanine perchlorate (DiI; Sigma, St Louis, MO, USA). For BMP2 adsorption, fluorescein isothiocyanate (FITC; Thermo Scientific, Rockford, IL, USA)-conjugated BMP2 (Huaan Co., Hangzhou, China) and DiI-labeled GO were mixed with phosphate-buffered saline (PBS) and incubated for 4 h at 4°C. The ratio of GO to BMP2 was 1:1 by weight. To determine the amount of BMP2 that should be loaded onto GO, 1 μg of BMP2 was added to 20 μL of PBS containing GO and incubated for 4 h at 4°C. BMP2 adsorbed onto GO was visualized using a laser scanning confocal microscope (IX81-FV1000 inverted microscope; Olympus). To confirm BMP2 adsorption onto GO, Fourier-transformed infrared spectroscopy (FTIR) was performed using a Nicolet 5700 spectrometer (Thermo Electron Scientific Instruments Corp., Madison, WI, USA) on pellets (10 mm in diameter), which were prepared by mixing 2 mg of samples with 100 mg of KBr in a mortar and pressing, to produce the pellets to be analyzed. Spectra were analyzed after baseline correction by

using the software EZ OMNIC (Nicolet Thermo Electron Scientific Instruments LLC, Madison, WI, USA).

Release kinetics of BMP2

The release profiles of BMP2 at various concentrations (10 μg/mL, 20 μg/mL, and 20 μg/mL) absorbed onto GO with or without hydrogels were determined by enzyme-linked immunosorbent assays (ELISAs; R&D Systems Inc., Minneapolis, MN, USA). Following incubation for 4 h at 4°C, an ELISA of the supernatant showed that all the BMP2 had adsorbed onto GO. Hydrogel was purchased from SaiYe Co. (Guangzhou, China). Hydrogel was prepared by mixing hydrogel (100 mg/mL) dissolved in PBS solution with 10 mL of that dissolved in a calcium chloride solution (6 mg/mL). The BMP2-loaded GO was resuspended in 0.5 mL of the hydrogel mixture and immersed in a 60 mm culture dish containing 1.5 mL of PBS. The dishes were then incubated at 37°C. At various time points, the supernatant was collected after continuous agitation with a shaker mechanically before removal of sample, and fresh buffer was added to the culture dishes. The concentration of BMP2 in the supernatant was determined using ELISA.

GO biocompatibility assay

The BMSCs and chondrocyte cultures were treated with the GO flakes with 10 μg/mL BMP2 for 1 day, 3 days, 5 days, 7 days, and 10 days. Cell viability was evaluated using the cell counting kit-8 (CCK8) assay as previously described. The absorbance of each sample was measured at a wavelength of 570 nm (n=5 for each group). Giemsa staining assay was performed to determine the activity of BMSCs and chondrocytes cultured with or without GO (BMP2: 20 μg/mL) according to the manufacturer's instructions. The number of F-actin-positive cells was also counted. Images of 30 different areas in each group were randomly selected, captured, and used in the calculations.

Flow cytometric characterization

BMSCs and chondrocytes were harvested by trypsinization and labeled with the following fluorescent dye: Hoechst33258 and Annexin V-FITC/propidine iodide (PI). Cell cycle staging and cell apoptosis were determined by using a Flow Cytometry Analysis Kit (Lianke, Hang Zhou, China). Labeling was performed for 30 min at 4°C in the presence of a blocking reagent (Lianke), followed by two washing steps using PBS. After washing and fixing, at least 10^4 cells were acquired and analyzed. Flow cytometric analysis was performed using a Becton Dickinson FACSCanto II.

Real-Time quantitative Polymerase Chain Reaction (RT-qPCR)

Total RNA was extracted using an RNA kit and protocol (GenePharma Co., Ltd., Shanghai, China). mRNA contained in 2 μg total RNA was reverse transcribed using a Transcriptor strand cDNA synthesis kit (GenePharma Co., Ltd.). PCR amplification was performed using a SYBRGreen PCR Master Mix (GenePharma Co., Ltd.) and the primers listed subsequently (Integrated DNA(deoxyribonucleic acid) Technologies [IDT], 300 nM). mRNA abundance was quantified using the threshold cycle method.

Collagen I: 5′-TGCTGCCTTTTCTCTCCTT-3′, 5′-AAGTGCTGGTAGGGAAT-3′;

Runx2: 5′-TGCTGGAGTGATGTGGTTTTCT-3′, 5′-CCCCTGTTGTGTTGTTTGGTAA-3′;

Aggrccan: 5′-GCATCCGAAACCCTGTAAC-3′, 5′-GGCGGTCAGCATCATAGTCC-3′;

OPN: 5′-CAAATACCCAGATGCTGTGGC-3′, 5′-TCCTGGCTGTCCACATGGAC-3′;

IRKA4: 5′-ACTTCTTGTACGAGGTGCCGCC-3′, 5′-GGGCAGGCCTGGGTCTGGCAGT-3′;

IKKα: 5′-CCGCTCGAGATGGACCGTTGCTACGATCC-3′, 5′-GGGGTACCTCAGTGCACCTGAGGCTG-3′;

IKKβ: 5′-GCCAGAAAACATCGTCCT-3′, 5′-CACCGTTCCATTCAAGTC-3′; and

NF-κB: 5′-GGAGGCATGTTCGGTAGTGG-3′, 5′-CCCTGCGTTGGATTTCGTG-3′.

In vivo experiments

The Zhejiang University Ethics Committee approved all experiments performed in rats. The guidelines followed for animals' welfare was Zhejiang University laboratory animal management regulations (03-2012). Four-week-old male Sprague Dawley rats underwent anterior cruciate ligament transection (ACLT) surgery on both knees as previously described.[28] Immediately after surgery, the animals were returned to their individual cages. Approximately 14 days after ACLT, intra-articular injections of PBS (10 μL/once, n=4), BMP2 alone (20 μg/mL, 10 μL, n=4), and BMP2-GO (20 μg/mL, 10 μL, n=4) were administered to the rats once per week. The rats were all sacrificed 4 weeks after ACLT. The distal femur was dissected, embedded in paraffin, and investigated by staining

with hematoxylin–eosin (HE), safranin, toluidine blue, and Masson and immunostaining.

OARSI scoring of cartilage

Semiquantitative histopathological grading was performed using the Osteoarthritis Research Society International (OARSI) scoring system.[29,30] Histological grading was performed in four areas: medial femoral condyle, medial tibial plateau, lateral femoral condyle, and lateral tibial plateau. The grades of four blinded observers for each section were averaged.

Histological and immunohistochemical analysis

Femur–tibia complexes were fixed in 4% formalin for 72 h. Then, the samples were decalcified in 9% formic acid for 2 weeks at room temperature. The samples were dehydrated across an ethanol gradient. Consecutive sections were stained with HE, safranin (Safranin O assay, Sigma S2255), toluidine blue (toluidine blue assay, Amresco 0672, Corporate Headquarters Amresco, LLC, Solon, OH, USA), and Masson (Masson assay, leagene YM-S1453).

Expression of NF-κB, IRAK4, IKKα, and IKKβ at the cartilage interface was analyzed by immunohistochemical staining. The sections were dewaxed in xylene and hydrated across an alcohol gradient. After blocking with 1% goat serum (1:100 dilution, Sigma), sections were incubated with primary antibodies against NF-κB (Abcam, Cambridge, UK), IRAK4 (Abcam), and IKKα/β (Abcam) overnight at 4°C. After washing with PBS three times, sections were incubated with a secondary antibody for 1 h at 37°C. Staining was developed in a 3,3′-diaminobenzidine (DAB) solution (Dako, Hamburg, Germany). Three trained observers examined the cartilage interface. The immunohistochemical sections were scored based on DAB percentage.

Statistical analysis

All experiments were repeated three times, and the data were expressed as the mean ± standard deviation. One-way analysis of variance (ANOVA) and the Student–Newman–Keuls post hoc test were employed to determine significance levels. *P*-values less than 0.05 and 0.01 were considered significant and highly significant, respectively. Statistical analysis was performed using SPSS 17.0 (SPSS Inc., Chicago, IL, USA).

Results

GO characterization

2D representation of GO images generated by AFM revealed that the GO flakes were of various sizes and were ~2 nm thick (Figure 1A). The height of the GO flakes (2 nm) also indicated that the GO is a bilayer structure. Furthermore, SEM showed that the GO flakes were irregularly shaped sheets (Figure 1B). The size distribution of the GO flakes based on their electric potential as measured by spectrophotometry ranged from 81.1 nm to 45,749.7 nm, with the most abundant size determined to be 1,598.5 nm (Figure 1C).

BMP2 adsorption onto GO flakes

After incubating DiI (red)-labeled GO and FITC (green)-conjugated BMP2 in PBS for 4 h, BMP2 was determined to have adsorbed onto the GO flakes (Figure 2A). This finding indicated that BMP2 protein effectively adsorbs onto the GO. We investigated the chemical ingredients involved in the GO and BMP2-GO adsorption by FTIR spectroscopy. A peak value of 1,800 cm^{-1} showed that carboxyl (C=O) was

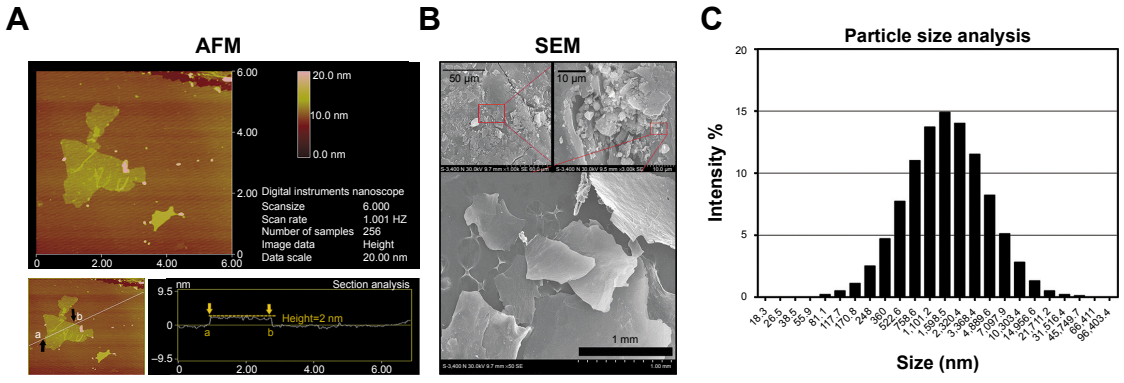

Figure 1 Characteristics of GO flakes.
Notes: (**A**) 2D representation of GO images as shown in AFM. GO flakes are of different sizes and are ~2 nm thick. (**B**) SEM analysis of GO flakes showing irregularly shaped sheets. (**C**) Size distribution of GO flakes, ranging from 81.1 nm to 45,749.7 nm. The most abundant size was 1,598.5 nm.
Abbreviations: AFM, atomic force microscopy; 2D, two-dimensional; GO, graphene oxide; SEM, scanning electron microscopy.

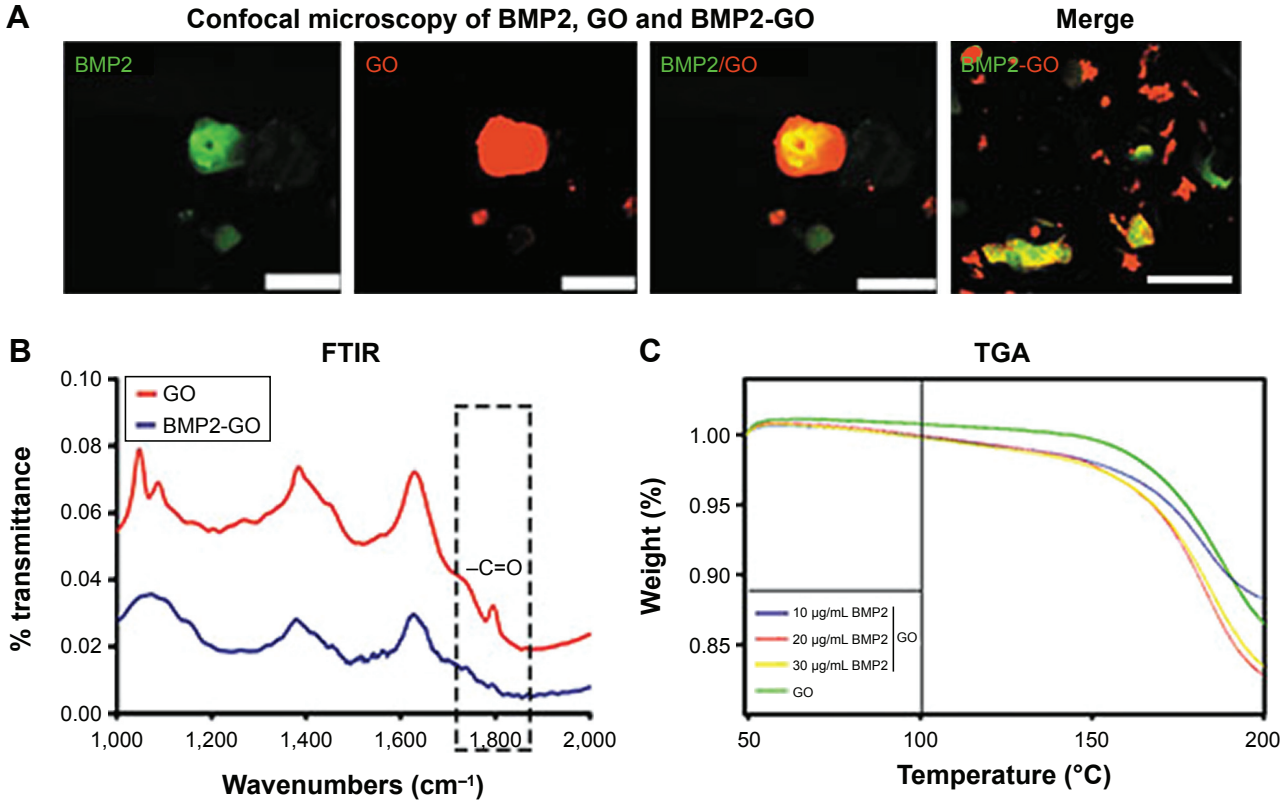

Figure 2 BMP2 adsorbed onto GO flakes.
Notes: (**A**) BMP2-FITC and GO-DiL were observed by laser confocal microscopy (bar =1 mm). (**B**) FTIR spectroscopy showing the chemical ingredients involved in the interaction between GO and BMP2-GO. A peak value of 1,800 cm^{-1} showed that carboxyl (C=O) was involved in the process of adsorption. (**C**) Thermal gravimetric analysis shows no differences between various concentrations of BMP2 but significant differences with GO from 50°C to 200°C.
Abbreviations: AFM, atomic force microscopy; BMP2, bone morphogenetic protein 2; FITC, fluorescein isothiocyanate; FTIR, Fourier-transformed infrared spectroscopy; GO, graphene oxide; TGA, thermogravimetric analyzer; GO-DiL,Graphene oxide–1,1-dioctadecyl-3,3,3,3-tetramethylindocarbocyanine perchlorate.

BPM2-GO and represents the key role of C=O in adsorption (Figure 2B). We further performed thermal gravimetric analysis of GO using various concentrations of BMP2 with GO (Figure 2C). The curve generated by thermal gravimetric analysis showed no differences between various concentrations of BMP2 from 50°C to 200°C.

BMP2 release

Various concentrations of BMP2 were mixed into the hydrogels with or without GO. Figure 3 shows that the cumulative release profiles of different BMP2 groups were slower in the BMP2 that was mixed into hydrogels and loaded with GO. The cumulative release profiles of different BMP2 groups are also presented in Figure 3. The observed rate of release using 20 μg/mL BMP2 release was apparently faster in reaching a 50% cumulative release compared to 10 μg/mL and 30 μg/mL BMP2. BMP2 was continuously released for at least 40 days at concentrations relevant for chondrocyte protection. This indicated that the application of BMP2 onto GO flakes is a suitable system for prolonged BMP2 release.

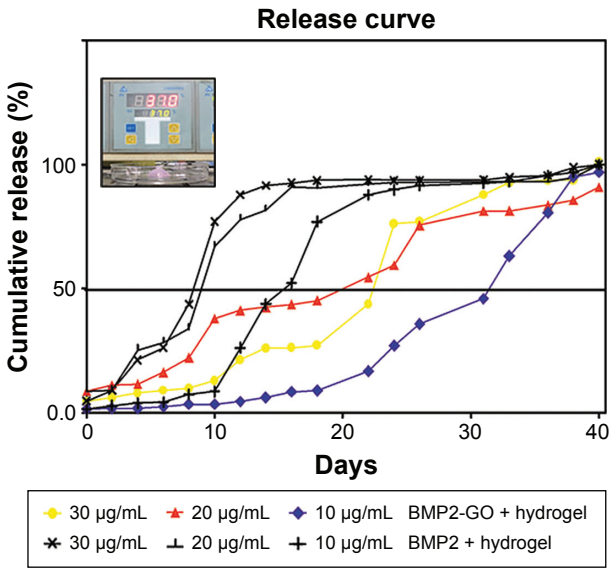

Figure 3 Cumulative release profiles of different BMP2 groups.
Notes: 20 μg/mL BMP2 release was apparently faster in reaching a 50% cumulative release compared to 10 μg/mL and 30 μg/mL BMP2. BMP2 was continuously released for at least 40 days. The inset image on the graph is the samples used in the cumulative release test on the constant 37°C.
Abbreviations: BMP2, bone morphogenetic protein 2; GO, graphene oxide.

Cell proliferation and viability with BMP2-GO

The proliferation and viability of BMSCs and chondrocytes cultured in BMP2 did not significantly differ from those of cells grown in BMP2-GO or GO ($P>0.05$; Figure 4A and B). After differentiation, periodic acid-Schiff (PAS) staining, alkaline phosphatase (ALP) staining, and Giemsa staining of BMSCs indicated that the differentiation effect of BMP2 was not affected by GO (Figure 4C and D). The differentiation and anti-inflammatory effect of BMP2-GO were more distinct than that of BMP2. The mRNA expression of IRAK4, IKKα, IKKβ, and NF-κB significantly decreased (Figure 4E and F). Immunohistochemical analysis of chondrocytes cultured in interleukin 1 (IL1) indicated that the protein expression levels of IRAK4, IKKα, IKKβ, and NF-κB decreased (Figure 4G).

Histological and immunohistochemical analyses in vivo

The animal model of ACLT was done in vitro (Figure 5). The histological features of cartilage after treatment with BMP2 are presented in Figure 5B. The articular cartilage of the control specimens after 4 weeks was thinner after ACLT, whereas thicker articular cartilage was observed in

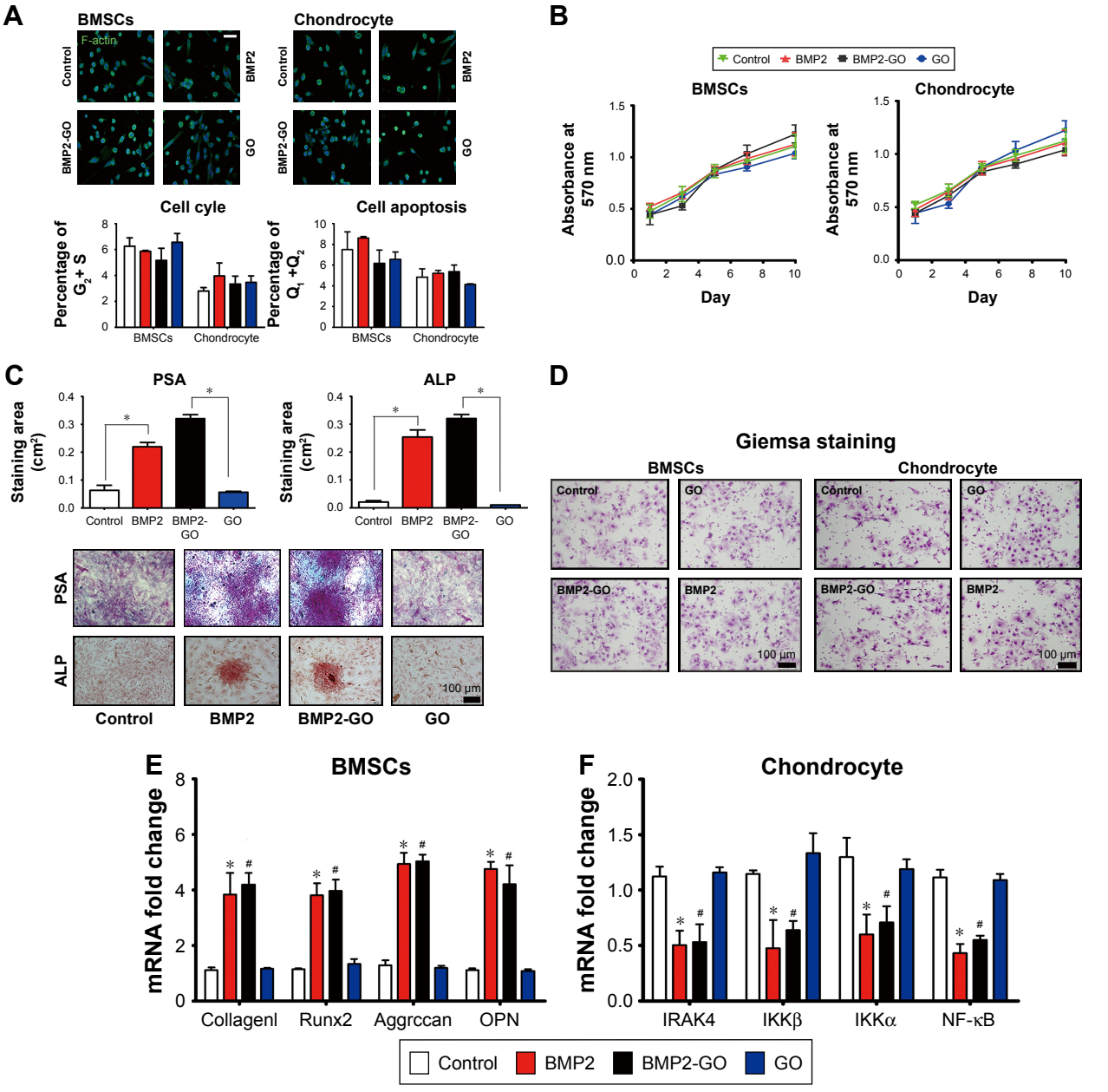

Figure 4 (*Continued*)

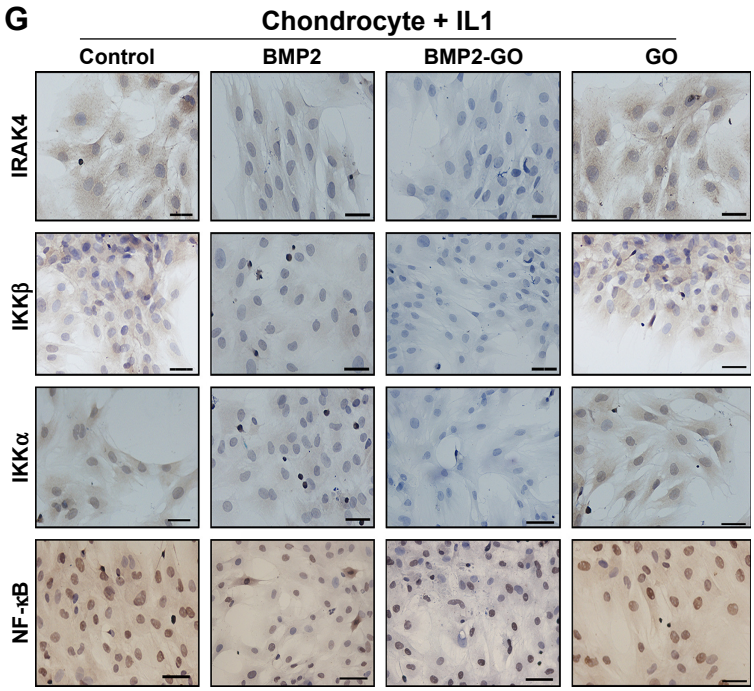

Figure 4 Cell proliferation, differentiation, and anti-inflammatory effect of GO.
Notes: (**A**) Cell morphology, cell cycle, and cell apoptosis of BMSCs and chondrocytes cultured in BMP2 show no significant differences from those of cells grown in BMP2-GO or GO ($P>0.05$; bar =100 μm). (**B**) Viability of BMSCs and chondrocytes cultured in BMP2 shows no significant differences from that of cells grown in BMP2-GO or GO ($P>0.05$). (**C** and **D**) After differentiation, PAS staining, ALP staining, and Giemsa staining of BMSCs showed that GO does not affect BMP2. (*$P<0.05$; bar =100 μm). (**E**) mRNA expression of BMSCs showed that GO improves cell differentiation. (*$P<0.05$, BMP2 compared with control and GO; #$P<0.05$, BMP2-GO compared with control and GO). (**F**) mRNA expression of chondrocytes showed that GO improves anti-inflammatory effect. (*$P<0.05$, BMP2 compared with control and GO; #$P<0.05$, BMP2-GO compared with control and GO). (**G**) Cell immunohistochemistry analysis of BMP2, GO, and BMP2-GO. Chondrocytes cultured in IL1 indicated that the protein expression levels of IRAK4, IKKα, IKKβ, and NF-κB decreased (bar =100 μm).
Abbreviations: BMSCs, bone marrow stem cells; BMP2, bone morphogenetic protein 2; GO, graphene oxide; IL, interleukin; CCK8, Cell Counting Kit-8; PSA, periodic acid-Schiff; ALP, alkaline phosphatase.

the BMP2-GO group. The immunohistochemical features of inflammatory cells in cartilage after treatment with BMP2 are presented in Figure 6A. More inflammatory cytokines were detected in the articular cartilage in the control group 4 weeks after ACLT, whereas a lower amount was observed in the BMP2 group. No inflammatory cytokines were detected in the articular cartilage of the BMP2-GO group 4 weeks after ACLT.

Quantitative assessment revealed significant differences between the control group with BMP2 and the BMP2-GO group ($P<0.05$, Figures 5C and 6B).

Efficacy of combining BMP2 with GO as an OA treatment

BMP2 with GO was intra-articularly administered to rats to determine whether it can control the progression of inflammation in OA. Approximately 4 weeks after surgery, compared to the OA group (control), OA rats treated with BMP2 and BMP2-GO showed significant differences in OARSI scores ($P<0.05$). Furthermore, the BMP2-GO group exhibited an enhanced therapeutic effect and a significantly lower OARSI score compared to the BMP2-only group ($P<0.05$), possibly due to the sustained release of BMP2 in the presence of GO (Figure 5D).

Discussion

In the present study, we developed a novel strategy for the treatment of OA, in which BMP2 combined with GO was applied, and the effect of combined BMP2-GO controlled release was compared to that of delivery of BMP2 alone. The present study has three major findings: first, there was a sustained release of BMP2 from GO for 40 days, which should be more therapeutically effective in protecting cartilage; second, GO sustained biocompatibility, as indicated in the results of the in vitro experiment; third, the combination of BMP2 and GO slowed the progression of inflammation and degenerative changes in OA.

Currently, a large variety of biomedical materials have been manufactured that can be used as carriers for tissue regeneration factors. Loading of carriers such as calcium phosphate cements,[31] titanium,[32] collagen,[33] silk,[34] and polylactic acid–polyglycolic acid[35] through simple adsorption merely resulted in an abrupt release of biological activity, which is apparently physiologically insufficient in resolving

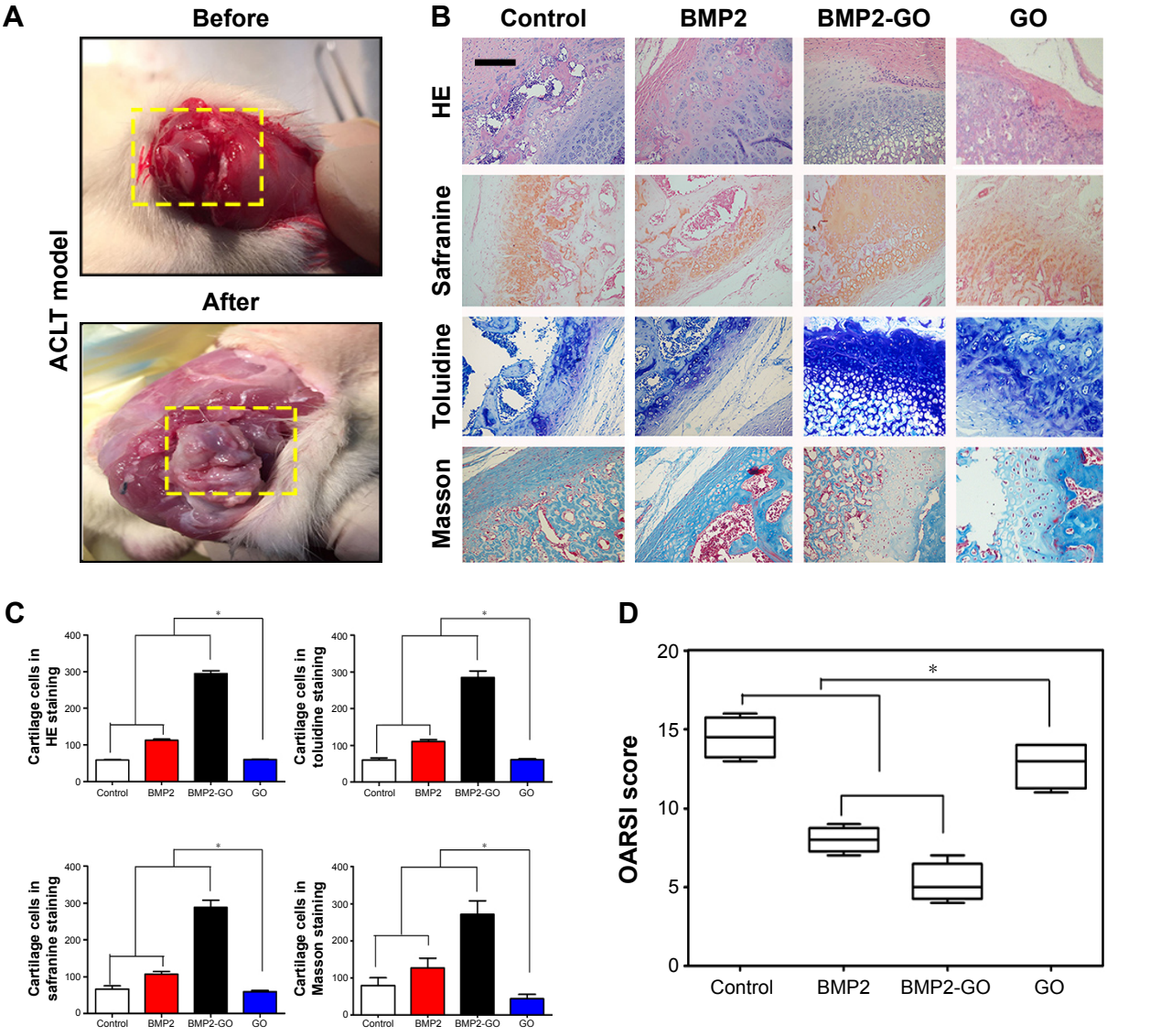

Figure 5 Histological analyses in vivo experiment.
Notes: (**A**) The ACLT model. (**B** and **C**) Histological analyses in vivo. Quantitative assessment reveals significant differences between the control group and GO group with BMP2 and the BMP2-GO group (*$P<0.05$; bar =100 μm). (**D**) OA rats treated with BMP2 and BMP2-GO show significant differences in OARSI scores (*$P<0.05$).
Abbreviations: ACLT, anterior cruciate ligament transection; BMP2, bone morphogenetic protein 2; GO, graphene oxide; HE, hematoxylin–eosin; OA, osteoarthritis; OARSI, Osteoarthritis Research Society International.

the inflammation associated with OA. Therefore, a significant feature for the suitability of these biomaterials is the ability to provide controlled release of the biologically active molecules.[36] Based on the literature, we analyzed the main reasons that GO could potentially serve as an excellent carrier of small molecule drugs, which can be summarized as follows: first, GO has a single or bilayer atomic layer structure. Good hydrophilicity allows its complete dispersal in water.[37] Thus, a larger specific surface area and surface activity combined with other dielectric materials facilitate more extensive distribution in a liquid substrate such as water.[38] The specific surface area of GO can reach 2,630 m^2/g,[39] whereas that of the common activated carbon is 1,500 m^2/g.[40] The larger specific surface area renders graphene as a carrier with high potential.[20] Second, the oxidation functional group increases the surface activity of GO.[41] This feature can be directly related to the dielectric material that is capable of electrostatic adsorption or bonding that yields a stable composite structure.[42,43] GO has the ability to self-assemble, similar to a surface active agent.[44] A continuous film tends to form a multilayer structure on a flat solid surface.[45,46] Most importantly, oxygen-containing groups on the surface of GO molecules may interact with hydroxyl groups of the BMP2 molecules through hydrogen bonding.[47,48] Third, the atomic layer framework of GO is of good mechanical strength,[49] which may provide mechanical support. At the molecular level, GO molecules are dispersed

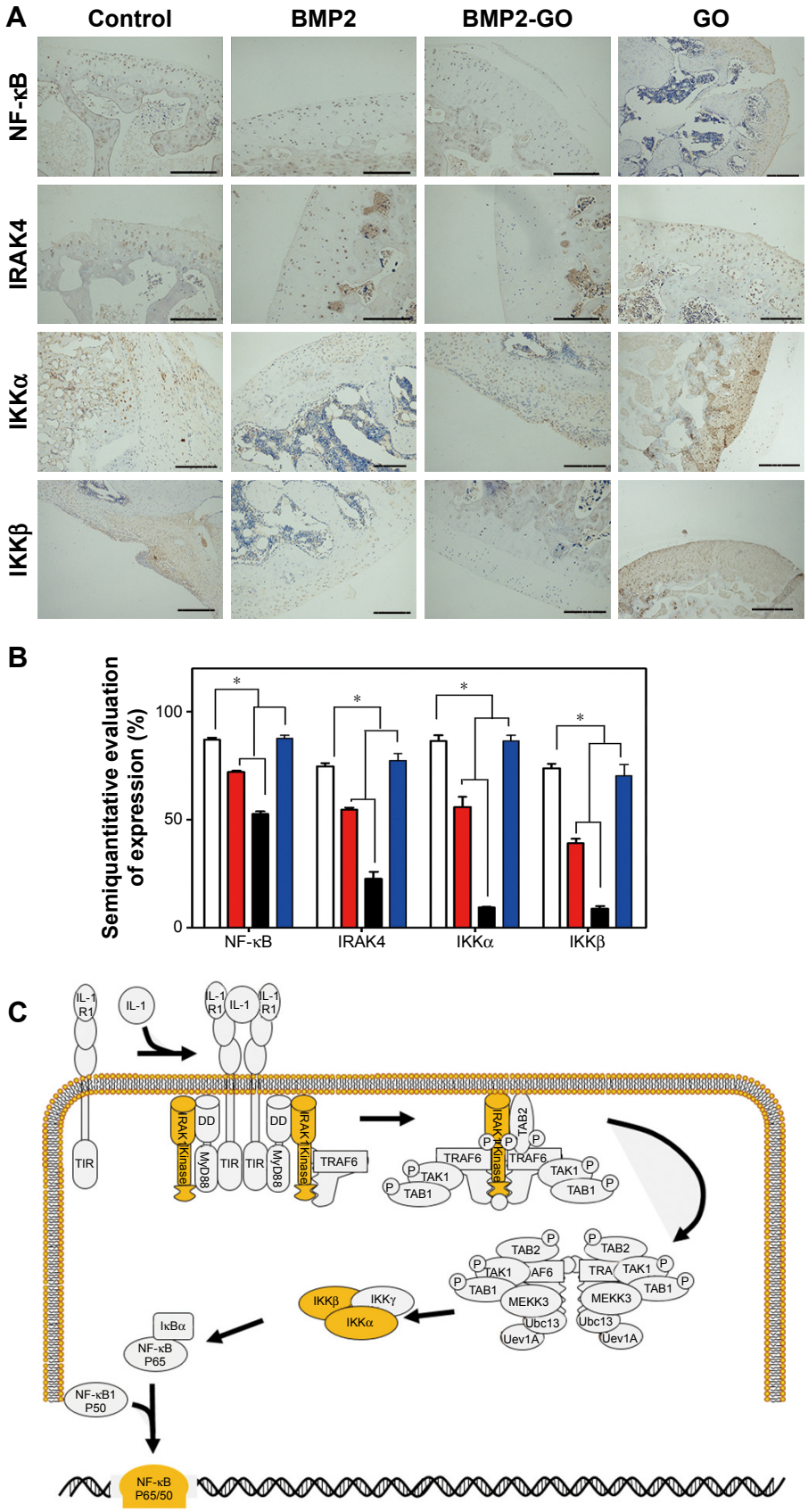

Figure 6 Immunohistochemistry analyses in vivo experiment.

Notes: (**A** and **B**) Immunohistochemistry analyses in vivo. Quantitative assessment reveals significant differences between the control group and GO group with BMP2 and the BMP2-GO group (*$P<0.05$; bar =100 μm). (**C**) GO influences the progression of cytokines such as IL-1a, IL-6, IL-10, and TNF-α via the NF-κB pathway.

Abbreviations: BMP2, bone morphogenetic protein 2; GO, graphene oxide; IL, interleukin.

across the matrix and interact with each other.[50] Tensile testing also indicated that tensile strength and Young's modulus significantly change during these interactions.[51,52]

Due to their small dimensions and highly developed surface,[53] GO molecules are chemically activated and may behave in an unpredictable manner after their introduction into cells. Thus, it is important to know the detailed mechanisms underlying their interactions with cells both in vitro and in vivo. It has been suggested that carbon particles with diameters <30 μm are deposited in tissues. Schinwald et al[54] suggested that GO molecules may have deposited into tissues and caused acute inflammatory reactions due to their extremely small diameter with large functional surface area. In contrast to previous studies, we observed the effect of GO deposition by HE staining. Due to the lack of conclusive findings on the side effects of GO molecules, we have no detailed evidence that would elucidate the mechanism underlying the interaction between graphene nanomaterials and cells,[55] and the hypothesis that GO nanoparticles cause the dysfunction of mitochondrial activity and increase the concentration of the intracellular reactive oxygen species was still controversial. Graphene can be considered as an immunostimulant for immunotherapy.[56,57] Most of the experiments, including biological response and safety tests,[58,59] have been conducted on graphene. Lymphocyte activation using a graphene antibody carrier was observed when therapeutic tumor-infiltrating lymphocytes were infused into a patient, which may have induced the tumor cell lysis and tumor regression.[60] Cells are generally administered to a patient after obtaining the appropriate subpopulation.[56] Understanding the precise mechanism of how this GO nanomaterial influences the immune system may potentially influence the application of graphene to the human body.

The observed prolonged release of BMP2 due to the presence of GO, compared to that of free BMP2, is likely due to the fact that an extended release of BMP2 would provide a continuous benefit for chondrocytes and articular cartilage. The long-term delivery of BMP2 helps cartilage cells avoid apoptosis and prevents the activation of inflammatory factors, which are required for treatment of OA. Blood samples should be collected from living animals to detect whether the drug reached the blood or was just localized in arthrosis. In addition, carbon atoms strongly interact with proteins in the plasma membrane, thereby resulting in changes in the spatial conformation of receptor proteins.[53] The downstream signaling pathways or receptors such as IL-1R may have been activated or inactivated.[54] Cytokines are controlled by regulatory transcription factors, which include NF-κB.[55] Researchers have proven that GO influences the progression of cytokines such as IL-1a, IL-6, IL-10, and TNF-α via the NF-κB pathway[56] (Figure 6C).

The size of a GO molecule is an important factor that affects its function as a drug carrier.[61] When the size of a GO molecule is too small, this may affect drug loading and the drug may be easily phagocytosed.[62] When the size of a GO molecule is too large, this may influence drug transport in the body.[63] The size of GO molecule investigated in this research did not affect drug loading and drug transport.

Conclusion

Current research investigations have focused on elucidating the mechanisms underlying the interaction between 2D GO molecules and cells. Graphene is a novel material whose properties facilitate a wide range of biological applications. However, because graphene occurs in various forms, its toxicology and biological interactions have not been fully elucidated. Information on its 2D carbon structure, particularly its biochemical responses at the tissue interface, thus require additional investigations. Utilization of graphene as a nanomaterial in biomedical applications should thus be established in the near future.

Acknowledgments

The authors obtained financial support from Zhejiang province key science and technology innovation team (Grant No 2013TD13), Zhejiang provincial natural science foundation of China (Grant No LQ16H160006), and National Science Foundation for Distinguished Young Scholars of China (Grant No 81601710).

Disclosure

The authors report no conflicts of interest in this work.

References

1. Sidorov VD, Pershin SB. [Rehabilitation of the patients with osteoarthritis]. *Vopr Kurortol Fizioter Lech Fiz Kult*. 2015;92(5):28–34. Russian.
2. Favero M, Ramonda R, Goldring MB, Goldring SR, Punzi L. Early knee osteoarthritis. *RMD Open*. 2015;1(suppl 1):e000062.
3. Shao JB, Ni CF, Duan PF, Jin YH. Preventive effects of different drugs on asymptomatic lower extremities deep venous thrombosis after artificial joint replacement: a mixed treatment comparison. *Am J Ther*. Epub 2016 Feb 1.
4. Quinlan E, Thompson EM, Matsiko A, O'Brien FJ, Lopez-Noriega A. Long-term controlled delivery of rhBMP-2 from collagen-hydroxyapatite scaffolds for superior bone tissue regeneration. *J Control Release*. 2015;207:112–119.
5. Sieker JT, Kunz M, Weissenberger M, et al. Direct bone morphogenetic protein 2 and Indian hedgehog gene transfer for articular cartilage repair using bone marrow coagulates. *Osteoarthritis Cartilage*. 2015;23(3):433–442.
6. Srinivasan PP, McCoy SY, Jha AK, et al. Injectable perlecan domain 1-hyaluronan microgels potentiate the cartilage repair effect of BMP2 in a murine model of early osteoarthritis. *Biomed Mater*. 2012;7(2):024109.

7. Molinari RW, Molinari C. The use of bone morphogenetic protein in pediatric cervical spine fusion surgery: case reports and review of the literature. *Global Spine J*. 2016;6(1):e41–e46.
8. Hussein KA, Choksi K, Akeel S, et al. Bone morphogenetic protein 2: a potential new player in the pathogenesis of diabetic retinopathy. *Exp Eye Res*. 2014;125:79–88.
9. La WG, Jin M, Park S, et al. Delivery of bone morphogenetic protein-2 and substance P using graphene oxide for bone regeneration. *Int J Nanomedicine*. 2014;9(suppl 1):107–116.
10. Lucarelli E, Beretta R, Dozza B, et al. A recently developed bifacial platelet-rich fibrin matrix. *Eur Cell Mater*. 2010;20:13–23.
11. Ortega-Oller I, Padial-Molina M, Galindo-Moreno P, O'Valle F, Jodar-Reyes AB, Peula-Garcia JM. Bone Regeneration from PLGA micro-nanoparticles. *Biomed Res Int*. 2015;2015:415289.
12. Wu G, Wang H, Qiu G, et al. [Preparation of vanilline cross-linked rhBMP-2/chitosan microspheres and its effect on mesenchymal stem cells]. *Zhonghua Yi Xue Za Zhi*. 2015;95(21):1691–1694.
13. Jeon O, Song SJ, Yang HS, et al. Long-term delivery enhances in vivo osteogenic efficacy of bone morphogenetic protein-2 compared to short-term delivery. *Biochem Biophys Res Commun*. 2008;369(2):774–780.
14. Fu YC, Chen CH, Wang CZ, et al. Preparation of porous bioceramics using reverse thermo-responsive hydrogels in combination with rhBMP-2 carriers: in vitro and in vivo evaluation. *J Mech Behav Biomed Mater*. 2013;27:64–76.
15. Tian HC, Liu JQ, Wei DX, et al. Graphene oxide doped conducting polymer nanocomposite film for electrode-tissue interface. *Biomaterials*. 2014;35(7):2120–2129.
16. Banerjee P, Sau S, Das P, Mukhopadhayay A. Optimization and modelling of synthetic azo dye wastewater treatment using graphene oxide nanoplatelets: characterization toxicity evaluation and optimization using Artificial Neural Network. *Ecotoxicol Environ Saf*. 2015;119:47–57.
17. Cheon YA, Bae JH, Chung BG. Reduced graphene oxide nanosheet for chemo-photothermal therapy. *Langmuir*. 2016;32(11):2731–2736.
18. Anis A, Mohammad AA, Hussain A, Ahmed SE. Reduced graphene oxide thin film on conductive substrates by bipolar electrochemistry. *Sci Rep*. 2016;6:21282.
19. Giordanelli I, Pose N, Mendoza M, Herrmann HJ. Conformal invariance of graphene sheets. *Sci Rep*. 2016;6:22949.
20. Rahmanian N, Hamishehkar H, Dolatabadi JE, Arsalani N. Nano graphene oxide: a novel carrier for oral delivery of flavonoids. *Colloids Surf B Biointerfaces*. 2014;123:331–338.
21. Song W, He C, Dong Y, et al. The effects of central metals on the photophysical and nonlinear optical properties of reduced graphene oxide-metal(II) phthalocyanine hybrids. *Phys Chem Chem Phys*. 2015;17(11):7149–7157.
22. Yu D, Ruan P, Meng Z, Zhou J. The structure-dependent electric release and enhanced oxidation of drug in graphene oxide-based nanocarrier loaded with anticancer herbal drug berberine. *J Pharm Sci*. 2015;104(8):2489–2500.
23. Wang SE, Si S. A fluorescent nanoprobe based on graphene oxide fluorescence resonance energy transfer for the rapid determination of oncoprotein vascular endothelial growth factor (VEGF). *Appl Spectrosc*. 2013;67(11):1270–1274.
24. Zhang M, Yu Q, Liang C, Liu Z, Zhang B, Li M. Graphene oxide induces plasma membrane damage, reactive oxygen species accumulation and fatty acid profiles change in *Pichia pastoris*. *Ecotoxicol Environ Saf*. 2016;132:372–378.
25. Guo F, Creighton M, Chen Y, Hurt R, Kulaots I. Porous structures in stacked, crumpled and pillared graphene-based 3D materials. *Carbon N Y*. 2014;66:476–484.
26. Kenry, Chaudhuri PK, Loh KP, Lim CT. Selective accelerated proliferation of malignant breast cancer cells on planar graphene oxide films. *ACS Nano*. 2016;10(3):3424–3434.
27. Chen YW, Liu TY, Chen PJ, Chang PH, Chen SY. A high-sensitivity and low-power theranostic nanosystem for cell SERS imaging and selectively photothermal therapy using anti-EGFR-conjugated reduced graphene oxide/mesoporous silica/AuNPs nanosheets. *Small*. 2016;12(11):1458–1468.
28. Yang PY, Tang CC, Chang YC, et al. Effects of tibolone on osteoarthritis in ovariectomized rats: association with nociceptive pain behaviour. *Eur J Pain*. 2014;18(5):680–690.
29. Fu SC, Cheuk YC, Hung LK, Chan KM. Limb Idleness Index (LII): a novel measurement of pain in a rat model of osteoarthritis. *Osteoarthritis Cartilage*. 2012;20(11):1409–1416.
30. Udo M, Muneta T, Tsuji K, et al. Monoiodoacetic acid induces arthritis and synovitis in rats in a dose- and time-dependent manner: proposed model-specific scoring systems. *Osteoarthritis Cartilage*. 2016;24(7):1284–1291.
31. Tahmasebi Birgani Z, Malhotra A, van Blitterswijk CA, Habibovic P. Human mesenchymal stromal cells response to biomimetic octacalcium phosphate containing strontium. *J Biomed Mater Res A*. 2016;104(8):1946–1960.
32. Cicciu M, Herford AS, Stoffella E, Cervino G, Cicciu D. Protein-signaled guided bone regeneration using titanium mesh and Rh-BMP2 in oral surgery: a case report involving left mandibular reconstruction after tumor resection. *Open Dent J*. 2012;6:51–55.
33. Osidak EO, Osidak MS, Sivogrivov DE, et al. Kinetics of BMP-2 release from collagen carrier: evaluation by enzyme immunoassay in the presence of plasma proteins. *Bull Exp Biol Med*. 2014;158(1):104–108.
34. Kim HJ, Kim UJ, Kim HS, et al. Bone tissue engineering with premineralized silk scaffolds. *Bone*. 2008;42(6):1226–1234.
35. Nie H, Soh BW, Fu YC, Wang CH. Three-dimensional fibrous PLGA/HAp composite scaffold for BMP-2 delivery. *Biotechnol Bioeng*. 2008;99(1):223–234.
36. Kuhfahl S, Schwarz E. A core domain of the BMP2 proregion is sufficient for the biogenesis of mature homodimeric growth factor. *Biol Chem*. 2015;396(3):215–223.
37. Chang G, Wang Y, Gong B, et al. Reduced graphene oxide/amaranth extract/AuNPs composite hydrogel on tumor cells as integrated platform for localized and multiple synergistic therapy. *ACS Appl Mater Interfaces*. 2015;7(21):11246–11256.
38. Cong HP, Chen JF, Yu SH. Graphene-based macroscopic assemblies and architectures: an emerging material system. *Chem Soc Rev*. 2014;43(21):7295–7325.
39. Yu JG, Yu LY, Yang H, et al. Graphene nanosheets as novel adsorbents in adsorption, preconcentration and removal of gases, organic compounds and metal ions. *Sci Total Environ*. 2015;502:70–79.
40. Martin-Gullon I, Font R. Dynamic pesticide removal with activated carbon fibers. *Water Res*. 2001;35(2):516–520.
41. Zeng T, Zhang H, He Z, Chen J, Song S. Mussel-inspired approach to constructing robust cobalt-embedded N-doped carbon nanosheet toward enhanced sulphate radical-based oxidation. *Sci Rep*. 2016;6:33348.
42. Chen X, Chen B. Direct observation, molecular structure, and location of oxidation debris on graphene oxide nanosheets. *Environ Sci Technol*. 2016;50(16):8568–8577.
43. Lingappan N, Jeong YT, Gal YS, Lim KT. Preparation and characterization of graphene/poly(diphenylamine) composites. *J Nanosci Nanotechnol*. 2013;13(5):3723–3727.
44. Creighton MA, Zhu W, van Krieken F, Petteruti RA, Gao H, Hurt RH. Three-dimensional graphene-based microbarriers for controlling release and reactivity in colloidal liquid phases. *ACS Nano*. 2016;10(2):2268–2276.
45. Lee S, Hong J, Koo JH, et al. Synthesis of few-layered graphene nanoballs with copper cores using solid carbon source. *ACS Appl Mater Interfaces*. 2013;5(7):2432–2437.
46. Veerapandian M, Seo YT, Shin H, Yun K, Lee MH. Functionalized graphene oxide for clinical glucose biosensing in urine and serum samples. *Int J Nanomedicine*. 2012;7:6123–6136.
47. Liu J. Interfacing zwitterionic liposomes with inorganic nanomaterials: surface forces, membrane integrity, and applications. *Langmuir*. 2016;32(18):4393–4404.
48. Burrs SL, Vanegas DC, Rong Y, et al. A comparative study of graphene-hydrogel hybrid bionanocomposites for biosensing. *Analyst*. 2015;140(5):1466–1476.

49. Rodrigues BV, Leite NC, Cavalcanti B, et al. Graphene oxide/multi-walled carbon nanotubes as nanofeatured scaffolds for the assisted deposition of nanohydroxyapatite: characterization and biological evaluation. *Int J Nanomedicine*. 2016;11:2569–2585.
50. Kim S, Yoo Y, Kim H, Lee E, Lee JY. Reduction of graphene oxide/alginate composite hydrogels for enhanced adsorption of hydrophobic compounds. *Nanotechnology*. 2015;26(40):405602.
51. Ghosh TK, Gope S, Mondal D, et al. Assessment of morphology and property of graphene oxide-hydroxypropylmethylcellulose nanocomposite films. *Int J Biol Macromol*. 2014;66:338–345.
52. Xiang C, Behabtu N, Liu Y, et al. Graphene nanoribbons as an advanced precursor for making carbon fiber. *ACS Nano*. 2013;7(2):1628–1637.
53. Wang X, Bai H, Shi G. Size fractionation of graphene oxide sheets by pH-assisted selective sedimentation. *J Am Chem Soc*. 2011;133(16):6338–6342.
54. Schinwald A, Murphy FA, Jones A, MacNee W, Donaldson K. Graphene-based nanoplatelets: a new risk to the respiratory system as a consequence of their unusual aerodynamic properties. *ACS Nano*. 2012;6(1):736–746.
55. Some S, Gwon AR, Hwang E, et al. Cancer therapy using ultrahigh hydrophobic drug-loaded graphene derivatives. *Sci Rep*. 2014;4:6314.
56. Jung JH, Cheon DS, Liu F, Lee KB, Seo TS. A graphene oxide based immuno-biosensor for pathogen detection. *Angew Chem Int Ed Engl*. 2010;49(33):5708–5711.
57. Liu Y, Luo M, Xiang X, et al. A graphene oxide and exonuclease-aided amplification immuno-sensor for antigen detection. *Chem Commun (Camb)*. 2014;50(20):2679–2681.
58. Syama S, Mohanan PV. Safety and biocompatibility of graphene: a new generation nanomaterial for biomedical application. *Int J Biol Macromol*. 2016;86:546–555.
59. Qiu Y, Guo F, Hurt R, Kulaots I. Explosive thermal reduction of graphene oxide-based materials: mechanism and safety implications. *Carbon N Y*. 2014;72:215–223.
60. Dudek I, Skoda M, Jarosz A, Szukiewicz D. The molecular influence of graphene and graphene oxide on the immune system under in vitro and in vivo conditions. *Arch Immunol Ther Exp (Warsz)*. 2016;64(3):195–215.
61. Frost R, Svedhem S, Langhammer C, Kasemo B. Graphene oxide and lipid membranes: size-dependent interactions. *Langmuir*. 2016;32(11):2708–2717.
62. Tran TH, Nguyen HT, Pham TT, et al. Development of a graphene oxide nanocarrier for dual-drug chemo-phototherapy to overcome drug resistance in cancer. *ACS Appl Mater Interfaces*. 2015;7(51):28647–28655.
63. Yuan Y, Zhang Y, Liu B, et al. The effects of multifunctional MiR-122-loaded graphene-gold composites on drug-resistant liver cancer. *J Nanobiotechnology*. 2015;13:12.